Desalination and Water Treatment
www.deswater.com

doi: 10.5004/dwt.2022.27951

245 (2022) 270–285
January

Plant based-biosynthesized silver doped zinc oxide for effective sonocatalytic degradation of malachite green: characterizations and optimization studies

Yin Yin Chan[a], Yean Ling Pang[a,b,*], Steven Lim[a,b], Chin Wei Lai[c], Ahmad Zuhairi Abdullah[d]

[a]*Department of Chemical Engineering, Lee Kong Chian Faculty of Engineering and Science, Universiti Tunku Abdul Rahman, 43000 Kajang, Selangor, Malaysia, Tel. +603-9086 0288; Fax: +603-9019 8868; emails: pangyl@utar.edu.my/ pangyeanling@hotmail.com (Y.L. Pang), yinyincyy95@gmail.com (Y.Y. Chan), stevenlim@utar.edu.my (S. Lim)*
[b]*Centre for Photonics and Advanced Materials Research, Universiti Tunku Abdul Rahman, 43000 Kajang, Selangor, Malaysia*
[c]*Nanotechnology and Catalysis Research Centre (NANOCAT), Institute of Advanced Studies (IAS), Universiti Malaya, 50603 Kuala Lumpur, Malaysia, email: cwlai@um.edu.my*
[d]*School of Chemical Engineering, Universiti Sains Malaysia, Nibong Tebal, 14300 Penang, Malaysia, email: chzuhairi@usm.my*

Received 22 June 2021; Accepted 29 October 2021

ABSTRACT

Sonocatalytic performance of silver doped zinc oxide (Ag-ZnO) nanoparticles synthesized using *Clitoria ternatea* Linn extract was optimized for the first time in the degradation of malachite green (MG) by using response surface methodology (RSM). A central composite design (CCD) model was successfully constructed to predict the sonocatalytic degradation efficiency in the studied range of operating variables including catalyst loading (0.75–1.50 g/L), initial MG concentration (500–1,250 mg/L), ultrasound power (40–80 W) and oxidant concentration (0.75–1.75 mM). The model was highly reliable in the evaluation of sonocatalytic degradation efficiency as it exhibited high coefficient of determination (R^2 = 0.9345) and high statistical significance (p-value < 0.0001). The maximum degradation efficiency of MG catalysed ultrasonically by Ag-ZnO was 89.21% after 15 min with 0.91% error as compared to the predicted value under the optimum conditions (500 mg/L initial dye concentration, 0.75 g/L of Ag-ZnO nanoparticles, 1.75 mM of sodium persulfate at 40 W of ultrasonic power). The excellent sonocatalytic performance was observed due to the enhancement in the availability of catalyst surface area, sufficient external energy as well as the addition of oxidant to induce more production of free radicals. In short, this work provides an insight and exposure for developing an optimized operating conditions towards the removal of hazardous organic dye pollutant.

Keywords: Silver-doped zinc oxide nanoparticles; Plant-mediated; Response surface methodology; Sonocatalytic degradation; Malachite green dye

1. Introduction

In this new era, the increase in the water pollution index is accelerated by the rapid growth of urbanization and industrialization. As reported by the World Health Organization (WHO), it was expected that at least half of the population will be staying in water-stressed region by 2025 due to the water contamination and shortage of clean water supply [1]. The discharge of industrial wastewater into the water bodies becomes a hot topic among the

* Corresponding author.

society due to the content of chemical waste especially organic dye which exhibits high persistency and stability in the environment and harmful to human being and the ecosystem [2]. In order to mitigate the problem of dye contamination, conventional techniques such as adsorption and biological methods are applied to remove organic pollutants. However, these methods are found to have several drawbacks such as the requirement of the additional adsorbent regeneration process and the nature of low biodegradable dye molecules [3].

Advanced oxidation processes (AOPs) such as electrochemical and photocatalytic methods have been developed to mineralize the organic compounds into less harmful products with the aid of reactive oxygen species (ROS) such as hydroxyl and superoxide radicals. In recent years, the catalytic degradation of organic substances under ultrasound irradiation has been widely studied. The presence of heterogeneous particles could enhance and accelerate the degradation of organic substances through sonocatalysis by reducing the energy required to form cavitation bubbles and providing electron–hole pair to generate free radicals [4].

In this case, ZnO is a promising sonocatalyst due to its stability under a wide range of operating conditions, non-toxicity properties as well as its good electrical and optical properties [5,6]. Although ZnO nanoparticle is a good semiconductor material, modification of pristine ZnO powder is commonly used to narrow the band gap energy and enhance the separation of electron–hole pair [7]. According to Reddy et al. [8], metal dopants could act as electron traps and lengthen the lifetime of the electron-hole pair. This can further enhance the formation of ROS and improve the degradation efficiency of organic compounds. Silver (Ag) is one of the promising dopant materials due to its effectiveness in the modification of nanocatalyst such as band gap narrowing and increment of surface area [9]. These factors are desired to improve the free radical generation and enhance the catalytic efficiency.

Accompanied by the invention of nanotechnology, the surface area and reactivity of nano-scaled particles are enhanced leading to the improvement in catalytic performance [10]. Biological approach is a novel technique invented to solve the problems of the conventional method in the preparation of nanoparticles especially the consumption of toxic chemicals. This method is also known as green synthesis because it is in line with the green chemistry principle. For example, biological approach uses safer solvents and renewable sources such as plant and microorganism to produce safer products [11]. The utilization of plant extract as bioresources in the green synthesis method is favourable instead of the microorganism due to the feasibility of the growing process in the environment without extra care is needed [12,13]. Besides, the majority of plant extracts are enriched with polyphenolic compounds which can act as bio-reductant in the synthesis of nanoparticles and also natural capping agents to stabilize the synthesized nanoparticles [14,15].

Recently, the generation of sulphate radicals in AOPs also garners the interest of researchers due to its good stability and performance in the degradation of organic substances [16]. In addition, the redox potential of sulphate radicals (2.5–3.1 V) is relatively higher than hydroxyl radicals (1.9–2.7 V) resulting in a stronger oxidizing ability which benefits catalytic degradation of organic molecules [17]. In this part, the presence of metal oxide is not only acts as a sonocatalyst but also facilitates the activation of persulfate anions to generate sulfate radicals. Hence, the combination of both catalyst and precursor of sulphate radicals can achieve a higher degradation efficiency of organic dye rather than the catalysis alone due to the acceleration of reactive free radical generation [18].

To the best of our knowledge, the sonocatalytic performance of green synthesized Ag-ZnO nanoparticles using *Clitoria ternatea* Linn extract was not reported previously. Hence, the catalytic performance of the synthesized Ag-ZnO in the degradation of MG dye was evaluated and compared with the pure ZnO nanoparticles in present work. *Clitoria ternatea* Linn was applied as the plant source to synthesis Ag-ZnO nanoparticles because it was reported to be enriched with phenolic acids and flavonoids which exhibit high reducing power [19]. Besides, the optimization of sonocatalytic degradation efficiency of MG dye using green synthesized Ag-ZnO was assessed using RSM modelling instead of conventional one-factor-at-a-time method. RSM is an effective and powerful statistical tool used for optimization by considering the interaction of operating variables in the design of experiments. In addition, the influences of several experimental variables on the outcomes can be evaluated simultaneously by the means of RSM approach leading to the reduction in laborious work [20].

2. Materials and methods

2.1. Chemicals and materials

Zinc nitrate hexahydrate (98% purity) as zinc precursor was obtained from Sigma-Aldrich while silver sulfate (purity ≥98.5%) as Ag source and benzoquinone (purity ≥98%) were bought from Merck. MG (99% purity) as sample dye was supplied from Friendemann Schmidt while sodium persulfate as oxidant was purchased from HmbG Chemicals. Methanol (purity ≥99.9%) and iso-butanol (purity ≥99.5%) were obtained from Emsure while ethylenediaminetetraacetic acid disodium (purity ≥99%) was purchased from Duksan. Distilled water was used throughout the study. All chemicals were used as received without further purification.

2.2. Green synthesis of pure and Ag doped ZnO nanoparticles

Plant extract was prepared prior to the green synthesis of ZnO nanoparticles. Firstly, *Clitoria ternatea* Linn as plant source was collected, washed and dried overnight in an oven at 70°C. Next, 3.0 g of dried *Clitoria ternatea* Linn was weighed and refluxed with 150 mL distilled water in a conical flask at 120°C for 6 h. The dark blue colored extract was left for cooling down and filtered using Whatman (No. 40) filter paper. The resulting filtrate was collected as plant extract for subsequent use in the fabrication of ZnO nanoparticles.

In the green synthesis of ZnO nanoparticles, 5.0 g of zinc nitrate was firstly placed in a teflon vessel containing

50 mL of *Clitoria ternatea* Linn extract. Then, the vessel was closed tightly and autoclaved at 70°C for 1 h. Next, the resulting product was calcined in a carbide furnace at 400°C for 2 h and solid ZnO nanoparticles was subsequently obtained in powder form. The biosynthesized ZnO nanoparticles was then ground using mortar pestle and labelled as Bio-ZnO. The steps were repeated for the preparation of 5 wt% Ag-ZnO by dissolving 0.10 g silver sulfate in the precursor solution containing plant extract and zinc nitrate. Commercial ZnO which was labelled as Com-ZnO was used as control in this study.

2.3. Catalysts characterization

The functional groups present in the prepared plant extract was identified through fourier transform infrared spectroscopy (FTIR) analysis utilizing a Nicolet IS10 system. The characterization of *Clitoria ternatea* Linn extract was also performed using a double-beam UV-Vis spectrophotometer. Besides, the field-emission scanning electron microscopy (FESEM) image of the analyzed ZnO nanoparticles was captured using a JEOL JSM-7601F. The morphology of Ag-ZnO particles was also characterized using transmission electron microscopy (TEM). In addition, the separation efficiency of electron–hole pair of the synthesized samples was determined through photoluminescence spectroscopy (PL) by the means of a Raman microscope (Renishaw inVia Raman Microscope) with an excitation wavelength of 325 nm. The zeta potential of ZnO samples was measured using a zetasizer (Malvern Zetasizer Nano ZSP) at the range of pH value between 2 and 12.

2.4. Sonocatalytic degradation study

The catalytic activity of the synthesized ZnO nanoparticles was investigated through the degradation of MG under ultrasound irradiation. The sonocatalytic performance evaluation was carried out using an Elma Transsonic series TI-H-5 ultrasonic bath with the operating settings at 45 kHz and 80 W of power. In a typical catalytic dye degradation experiment, a specified amount of catalyst was dispersed in dye solution followed by the addition of oxidant. In this experiment, 1 g/L of ZnO nanoparticles and 1 mM of sodium persulfate were added into the 100 mL of 500 mg/L MG solution. The ultrasonic bath was then switched on immediately and every 5 mL aliquot of dye was collected at regular time intervals in which the reaction was lasting for 60 mins. The sample was filtrated to separate the catalysts before subjected to liquid sample analysis. A single-beam UV-vis spectrophotometer (PG Instruments T60) was used to monitor the catalytic performance of ZnO nanoparticles in dye degradation by measuring the concentration of dye samples collected at a maximum absorbance wavelength of 617 nm. The degradation efficiency of dye was evaluated using Eq. (1) where C_0 is the initial dye concentration and C_t is dye concentration at time t.

$$\text{Degradation efficiency} = \frac{C_0 - C_t}{C_0} \times 100\% \quad (1)$$

In this study, the dye solution was also exposed to the ultrasound irradiation in the absence of both catalyst and oxidant in order to study the effect of sonolysis on the degradation of aqueous MG. Besides, the adsorption of dye molecules onto ZnO nanoparticles was studied under the condition without ultrasonic irradiation. The experiment was also carried out in the absence of oxidant under ultrasound irradiation in order to investigate the individual effect in dye degradation.

2.5. RSM modelling

In this study, RSM was applied to determine the optimal operating condition of the MG degradation with the minimum experiment runs. By the means of RSM, time saving can be achieved as compared to one-factor-at-a-time approach as the number of experiment sets was reduced significantly. CCD was applied for the experimental optimization as CCD model established well-fitting on a quadratic surface. In addition, CCD model was employed to evaluate the individual impact of process factors on the dye degradation efficiency and their interactions between each other. Design Expert Version 11 Software was used to develop the experimental matrix of CCD model. The number of experiment runs needed, N was calculated using Eq. (2) where k is the number of experimental variables and C_p is the number of central points.

$$N = 2^k + 2k + C_p \quad (2)$$

By using CCD model, 4 experimental parameters including catalyst loading (A), initial dye concentration (B), ultrasound power (C) and oxidant concentration (D) were selected as independent variables for the process optimization. These factors were coded as –1 and +1 to represent the low level and high level, respectively. Table 1 shows the codes and levels of factors selected for optimization study.

After collecting the experimental data, a second-order polynomial modelling as shown in Eq. (3) was applied to express the model performance where R is the response of the experiment (i.e., dye degradation efficiency), β_o is the constant coefficient, β_i, β_{ii} and β_{ij} are interaction coefficients of linear, quadratic and second-order terms, x_i and x_j are independent variables and ε is the error.

$$R = \beta_o + \sum_{i=1}^{k} \beta_i x_i + \sum_{i=1}^{k} \beta_{ii} x_i^2 + \sum_{i=1}^{k-1} \sum_{j=1}^{k} \beta_{ij} x_i x_j + \varepsilon \quad (3)$$

Table 1
Experimental factors with their unit, code and level

Factors	Code	Levels	
		–1	+1
Catalyst loading, g/L	*A*	0.75	1.50
Initial dye concentration, mg/L	*B*	500	1250
Ultrasound power, W	*C*	40	80
Oxidant concentration, mM	*D*	0.75	1.75

The statistical significance of the model at 95% confidence level was then evaluated using the analysis of variance (ANOVA) technique. *F*-test was applied to determine adequacy of the developed model in the prediction of a variation in experimental data without exceeding the confidence limit. In addition, the regression coefficient (R^2) and the lack of fit were important to analyse the feasibility of the resulting model. On the point of view, a strong R^2 value and less significant lack of fit were desired to determine the validity of the designed model. In addition, three dimensional response surface and contour plots were generated to identify the impact of each factor and the interactive between parameters.

2.6. Optimization of sonocatalytic degradation

The optimum condition for the sonocatalytic degradation of MG dye was determined using the results obtained from RSM and confirmed via experiment. The resulting samples were measured using double beam UV-Vis spectrophotometer to study the decomposition of MG molecules under ultrasound irradiation. In addition, chemical oxygen demand (COD) analysis was conducted with the aid of test kits available commercially to confirm the mineralization of dye in the presence of Ag-ZnO nanoparticles under ultrasonic irradiation in which the COD level was measured using a colorimeter (Hach DR 3900). Furthermore, radical scavenging test was conducted to identify the radicals present in the reaction system which were responsible in the degradation of MG dye. In this experiment, chemical scavenger was added into MG dye solution at a constant 1/500 molar ratio of MG to scavenger to quench particular radicals. [16] Benzoquinone (BQ), methanol (MetOH), isobutanol (IBA) and ethylenediaminetetraacetic acid disodium (EDTA-2Na) were used as chemical scavengers for superoxide radicals, sulphate radicals, hydroxyl radicals only and holes respectively.

2.7. Reusability study of Ag-ZnO as sonocatalyst

The reusability of Ag-ZnO was investigated by recovering the catalyst from the treated solution through centrifugation. The obtained Ag-ZnO sample was then washed at least three times using distilled water. Next, the catalyst was dried at 80°C overnight in an oven. After completion of the recovery process, the sonocatalytic performance of the reused Ag-ZnO was investigated by studying the degradation efficiency of MG under similar optimum condition. In this part, the steps were repeated to observe the stability of catalyst for up to 5 catalytic cycles. Besides, X-ray diffraction (XRD) patterns of the original and spent catalyst were determined using Shidmazu XRD-6000 with Cu-Kα radiation to determine the crystallinity structure.

3. Results and discussion

3.1. Characterization

Fig. 1a shows the FTIR spectrum of *Clitoria ternatea* Linn extract, uncalcined Ag-ZnO and calcined Ag-ZnO. Both the plant extract and uncalcined Ag-ZnO exhibited a characteristic peak in the range of 3,600–3,000 cm^{-1} which was

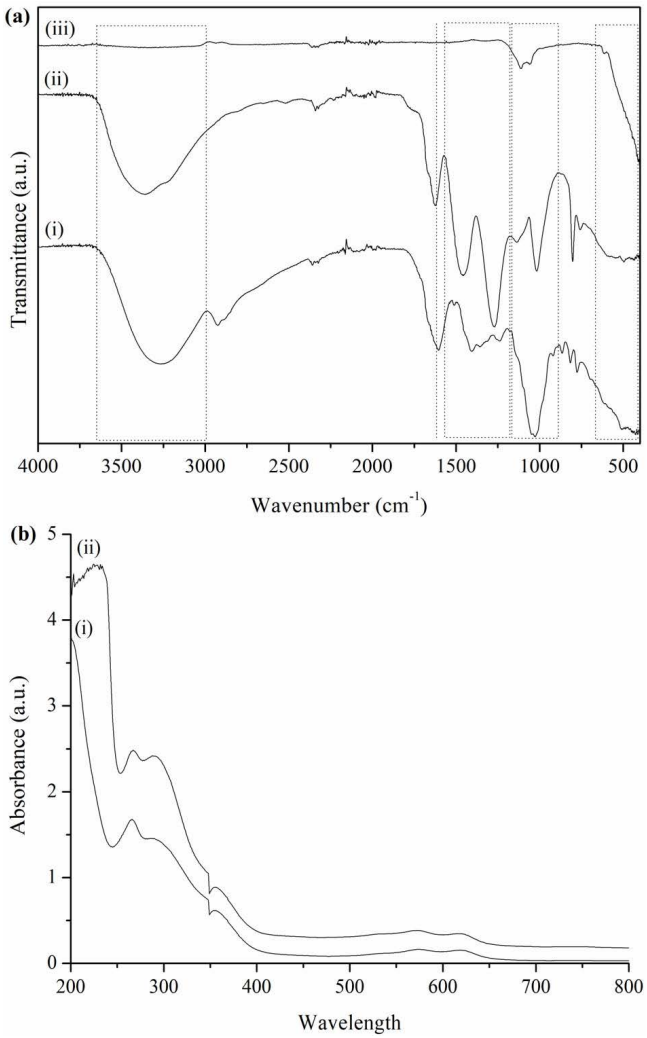

Fig. 1. (a) FTIR of (i) *Clitoria ternatea* Linn extract, (ii) uncalcined Ag-ZnO and (iii) calcined Ag-ZnO and (b) UV-Vis spectra of (i) *Clitoria ternatea* Linn extract and (ii) Ag-ZnO.

assigned to the R-O-H stretching while the band observed at 1,600 cm^{-1} was related to the C=O bond of ketones [15,21]. The presence of a broad peak in the range of 1,550–1,200 cm^{-1} was identified as the characteristic peaks of C=C and C–O contributed from aromatic compounds. These peaks depicted the presence of polyphenolic compounds such as flavonoids and alkaloids in the plant extract [22]. The peak presented in the range of 1,200 and 900 cm^{-1} was referred to functional groups of C=O and C=N originated from the carboxylic acids of flavonoids and phenolic compounds [23]. By comparing the FTIR spectra of plant extract and uncalcined Ag-ZnO nanoparticles, the involvement of phytochemicals in the formation of ZnO nanoparticles was confirmed. The peaks of organic impurities were found to disappear after calcination of Ag-ZnO due to the decomposition of organic residues at high temperature.

Fig. 1b presents the UV-Vis spectrum of *Clitoria ternatea* Linn extract. Both peaks appeared at 266 and 354 nm were associated with the presence of flavonoids and flavones in the *Clitoria ternatea* Linn extract [12,14]. These

two peaks were also observed in the UV-Vis spectrum of Ag-ZnO. The findings were in a good agreement with the results obtained in FTIR analysis which confirmed the presence of the bioactive molecules in the extract and involvement of biomolecules in the synthesis of ZnO nanoparticles. According to Thomas et al. [15], the presence of hydroxyl groups in plant extract was responsible in the green synthesis process as reductant owing to the electronegative behaviour of oxygen atom. The hydroxyl groups of flavonoids present in the *Clitoria ternatea* Linn extract are attached to the metal salt and reduced it to ZnO nanoparticles.

Fig. 2 presents the surface morphology of the analysed ZnO samples. The FESEM images depicted that Com-ZnO was found in cylindrical shapes while both Bio-ZnO and Ag-ZnO exhibited spherical shapes. It is noteworthy that Bio-ZnO had a comparatively smaller particle size in the range of 20–33 nm than Com-ZnO. This was owing to the involvement of natural capping agents present in the *Clitoria ternatea* Linn extract during the green synthetic route of ZnO nanoparticles which obstructed the continuous growth of particle and stabilize the synthesized ZnO powder [24]. This resulted in the formation of ZnO nanoparticles with smaller size and better shape regularity.

The findings also revealed that the incorporation of Ag into the ZnO matrix caused a slight decrement in the particle size which was measured in the range of 13–27 nm. The reduction in particle size was occurred due to the diffusion of Ag in ZnO lattice during the fabrication process which distorted and restricted the crystal growth. Besides, an increment in the particle agglomeration was observed due to the substitution of Ag impurities near the grain boundaries of ZnO nanoparticles. The effect of metal doping on the surface morphology of ZnO nanoparticles was further supported by Sukriti et al. [25]. The particle size of Ag-ZnO evaluated in TEM image was found to be consistent with the results obtained through FESEM. The dark spot observed in TEM image was found to be Ag dopants due to its high atomic number than Zn and O particles [5]. The results showed good distribution of Ag impurities over the ZnO matrix. Besides, the darker region

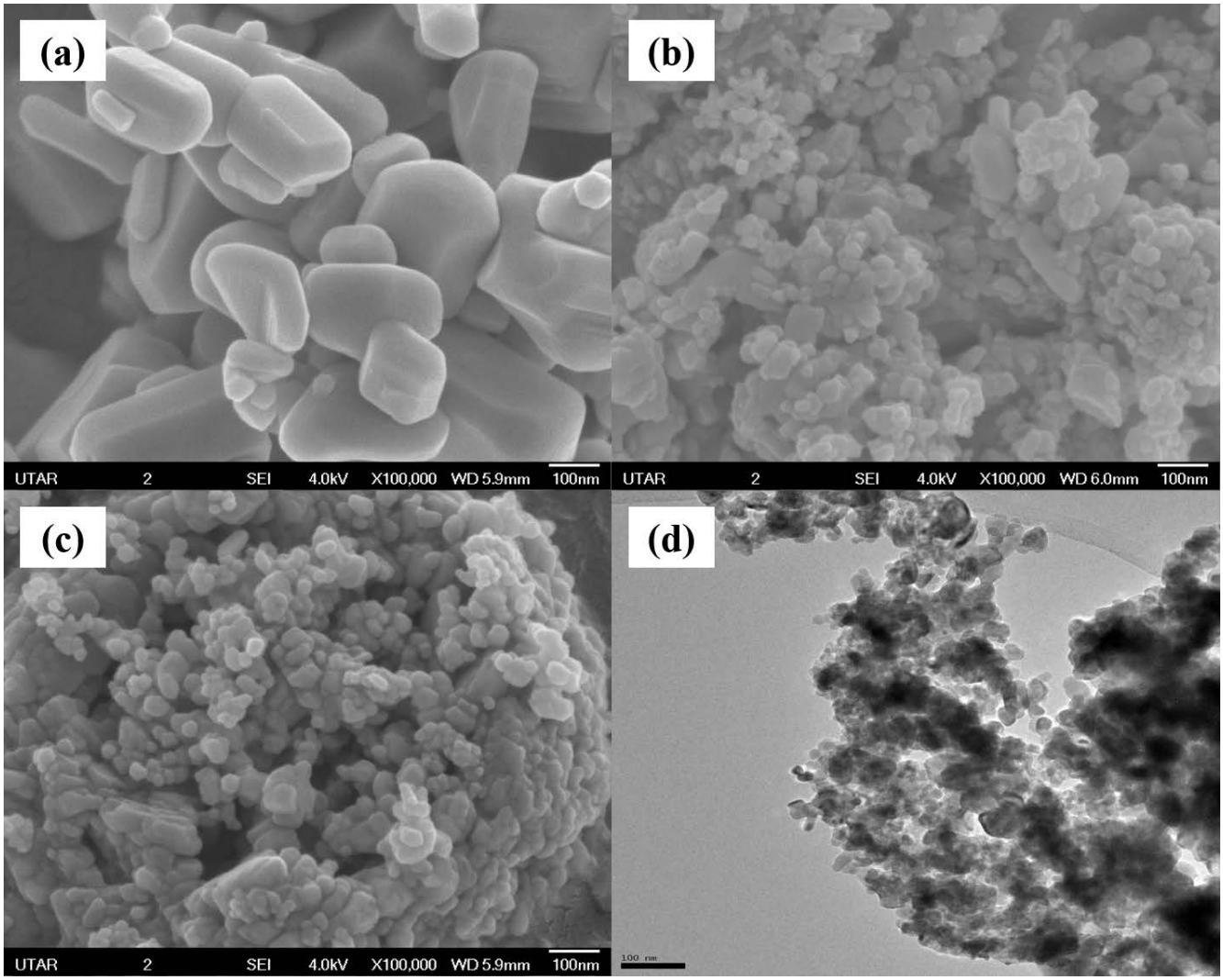

Fig. 2. FESEM images of (a) Com-ZnO, (b) Bio-ZnO, (c) Ag-ZnO at x100,000 magnification and (d) TEM image of Ag-ZnO at x19,500 magnification.

of the TEM image indicated the agglomeration of Ag-ZnO nanoparticles as observed in FESEM image.

Fig. 3 shows the PL spectra of Bio-ZnO and Ag-ZnO at 325 nm excitation wavelength. The results obtained from PL analysis were correlated to the recombination efficiency and lifetime of the generated electron-hole pairs. According to Chinnathambi [26], the recombination of charge carriers would release energy as photoluminescence. Hence, the quenching of PL emission peak intensity indicated that the sample exhibited good electron-hole pair separation efficiency and a low recombination rate. It is noteworthy that the PL emission intensity of Ag–ZnO was dramatically lower than that of Bio-ZnO. This resulted from the introduction of Ag dopant into ZnO matrix which as an electron trapping site hindering the recombination of electron-hole pair. Thus, the lifetime of the electron-hole pair was prolonged leading to an improvement in the catalytic activity of Ag-ZnO. In other words, the weaker recombination of the electron-hole pair increased the chance of radical generation during sonocatalytic oxidation process. As discussed by Mehrizad et al. [27], ultrasound irradiation triggered the formation of electron-hole pair by exciting the electron of the catalyst from the valence band to the conduction band. The negatively charged electron would react with dissolved oxygen in the liquid medium to form superoxide radical while the positively charged hole would react with water molecules to generate hydroxyl radical. In this case, Ag-ZnO with quenched PL emission peaks exhibited better electron-hole pair separation efficiency leading to higher electron concentration in the valence band under ultrasound irradiation. Hence, the generation of ROS was enhanced due to the prolonged electron–hole pair lifetime. Therefore, greater amount of strong oxidative radicals was generated which played an important role to oxidize the organic dye molecules through sonocatalytic process.

3.2. Catalytic performance of ZnO nanoparticles

Fig. 4 compares the dye removal efficiencies among Com-ZnO, Bio-ZnO and Ag-ZnO through adsorption and sonocatalysis processes. The findings reveal that Ag-ZnO exhibits the highest adsorption capabilities as its dye removal efficiency (24.22%) as compared to Com-ZnO (5.98%) and Bio-ZnO (9.15%). This was owing to the smallest particle size of Ag-ZnO powder as observed through FESEM images among the analysed samples. Jothi Ramalingam et al. [28] confirmed that the surface area of a nanomaterial was inversely correlated to the particle size.

Besides, the adsorption of MG in the presence of Com-ZnO was found to be the lowest removal efficiency as compared to Bio-ZnO and Ag-ZnO. This might be due to the cationic nature of MG and the natural solution pH detected was about 3.1, which was lower than the zero-point charge (pH_{zpc}) of Com-ZnO. According to the results of zeta potential measurement, the pH_{zpc} of Com-ZnO, Bio-ZnO and Ag-ZnO were found to be 6.4, 2.6 and 2.2, respectively. At the condition of pH values below pH_{zpc}, the surface of ZnO nanoparticles was protonated and positively charge due to the excessive amount of H^+ ions present in the solution. In other words, the presence of OH^- ions would contribute to the negative surface charge of ZnO samples at pH values above pH_{zpc} [29]. Therefore, the positively charged Com-ZnO would repel the cationic dye molecules from occupying the active sites of ZnO samples at solution pH lower than pH_{zpc} [30]. In contrast, the adsorption of MG was favourable in the presence of Bio-ZnO and Ag-ZnO. This was because the solution pH was higher than the pH_{zpc} of Bio-ZnO and Ag-ZnO. It was anticipated that there was a force of electrostatic attraction appeared between the cationic dye molecules and negatively charged ZnO nanoparticles [31]. Hence, Ag-ZnO the best dye removal efficiency through the adsorption process due to the most negatively charged behavior and the highest specific surface area available for the attachment of MG molecules.

In addition, Ag-ZnO also performed the highest catalytic activity in the dye degradation under ultrasonic irradiation as compared to the pristine ZnO samples. This was attributed to the band gap narrowing effect through the

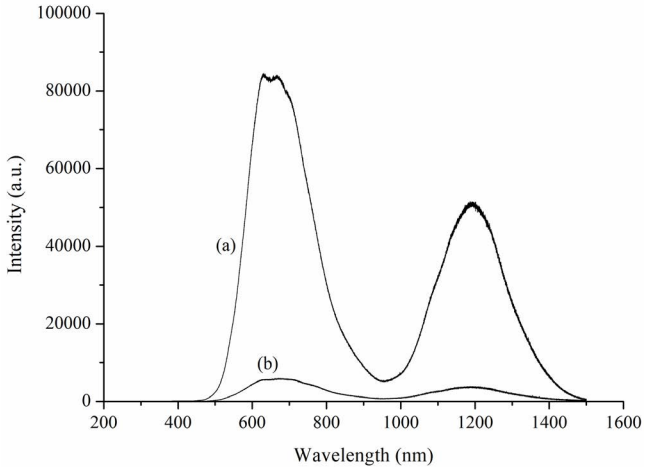

Fig. 3. PL spectra of (a) Bio-ZnO and (b) Ag-ZnO.

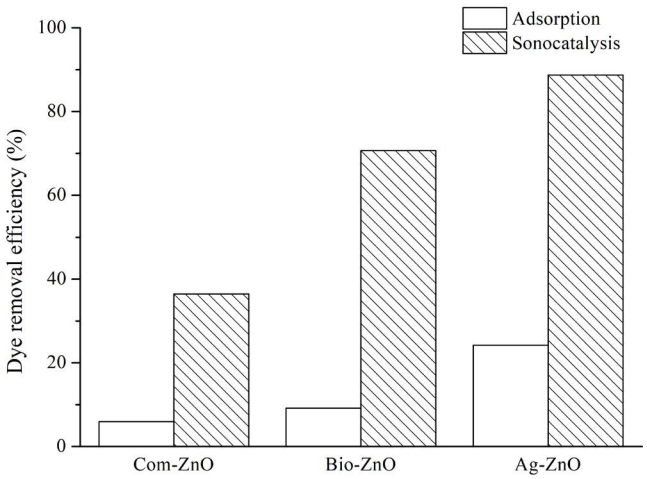

Fig. 4. Comparison of dye removal efficiency among Com-ZnO, Bio-ZnO and Ag-ZnO through adsorption and sonocatalysis processes. (Initial dye concentration = 500 mg/L, catalyst loading = 1 g/L, concentration of oxidant = 0 mM, ultrasonic power = 80 W, time taken = 60 min).

doping of Ag into ZnO lattice as discussed in the previous work [32]. According to Reddy et al. [8], the reduction in band gap was related to the presence of impurity energy levels between the conduction band and the valence band in the metal-doped substance. Therefore, Ag-ZnO exhibited the highest degradation efficiency through the sonocatalysis process.

Fig. 5 illustrates the degradation efficiencies of MG under different conditions. Sonolysis occurred due to the acoustic cavitation of microbubbles in the aqueous dye medium. This phenomenon led to the creation of hotspot and pyrolysis of water molecules into ROS such as hydrogen and hydroxyl radicals. These radicals were responsible for the oxidation of MG molecules [33]. However, the degradation efficiency of sonolysis was only 8.43% due to the limited generation of ROS and these ROS might react to form hydrogen peroxide other than the mineralization of MG molecules [27].

The degradation efficiency was improved to 71.89% in the presence of sodium persulfate as oxidant under ultrasonic irradiation. This was attributed to the presence of sulphate ions to facilitate the decomposition of MG molecules through chains of reaction. The sulphate ions contributed by the sodium persulfate could be converted into sulphate radicals under direct ultrasound irradiation which possessed a strong oxidizing ability in the degradation of MG. Besides, sulphate radicals could be formed through the reaction between sulphate ions and hydroxyl radicals. The sulphate radicals could also react with water molecules to enhance the formation of hydroxyl and hydrogen radicals, led to a better dye degradation efficiency [18].

On the other hand, the presence of Ag-ZnO nanoparticles in the system improved the dye degradation efficiency to 84.49%. This was because the nucleation sites for cavitation bubbles formation increased due to the surface roughness of the heterogeneous catalyst that led to the enhancements in the bubble cavitation and radical generation [33]. In addition, photon emission during the sonoluminescence phenomenon could also trigger the formation of electron-hole pairs [34]. Water and oxygen molecules adsorbed on the sonocatalyst surface were then converted into hydroxyl and superoxide radicals through the reaction route with electron–hole pair generated [2]. As consequence, the degradation efficiency of dye was strengthened due to the formation of numerous ROS.

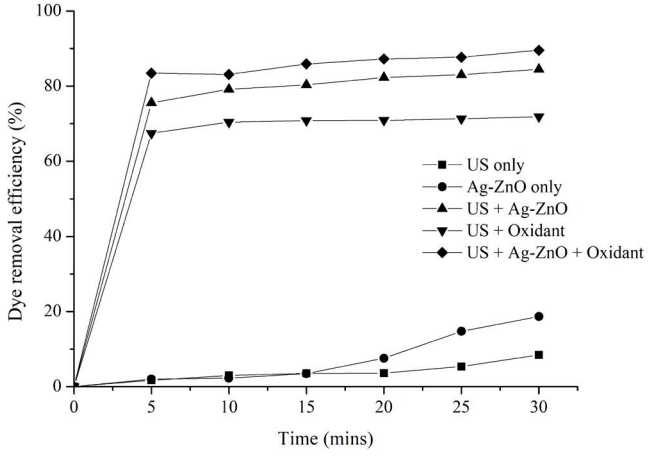

Fig. 5. Degradation efficiency of MG in different conditions in the presence of Ag-ZnO. (Initial dye concentration = 500 mg/L, catalyst loading 1 g/L, oxidant = sodium persulfate, oxidant concentration = 1 mM, ultrasonic power = 80 W, ultrasonic irradiation time = 30 min).

Other than the sonocatalysis mechanisms, the improvement of dye removal efficiency was owing to the enhancement in the mass transfer rate under ultrasound irradiation. Microjet-induced ultrasound shock wave might create turbulence in the dye solution which inhibited the aggregation of nanoparticles. Moreover, ultrasound would eliminate the products of dye degradation from the surface of sonocatalyst continuously through vibration induced by the ultrasound wave. Hence, the dye adsorptive surface area could be hindered under ultrasound irradiation and the dye removal efficiency could be enhanced [33].

Fig. 5 also shows that the system exhibited the highest dye degradation efficiency (89.59%) in the presence of both Ag-ZnO nanoparticles and sodium persulfate under ultrasound irradiation. This was due to the generation of ROS such as hydroxyl and superoxide radicals through the formation of electron–hole pair on the sonocatalyst [35]. In addition, Ag-ZnO also played an important role in the activation of persulfate ions by the excited electron, leading to the conversion to sulphate radicals [17]. The transfer of an electron to persulfate ions would also suppress the recombination of electron–hole pair on the surface of the catalyst, resulting in the improvement in the generation of reactive free radicals [16]. Hence, the enormous amount of radicals present in the reacting medium accelerated the oxidation of MG molecules into less small molecules and eventually form water and carbon dioxide molecules.

3.3. RSM modelling and optimization of sonocatalytic MG degradation efficiency

Table 2 presents the CCD design of the experiment together with the predicted and actual values of degradation efficiency. The results showed that the degradation efficiency obtained in this study was in the range of 28.24% to 89.49%. Eq. 4 shows the equation of this CCD model in terms of coded factors obtained via regression analysis after omitting the insignificant terms.

$$\text{Degradation efficiency (\%)} = 61.47 + 3.11A - 13.58B + 10.62D + 2.88BC \quad (4)$$

Fig. 6 illustrates the plot of predicted and actual outcomes of the response in this study. The findings showed that the experimental data were fitted well with the designed model. The statistical analysis revealed that this model exhibited a high R^2 value of 0.9345, indicated a high correlation between the predicted and actual values of MG degradation efficiency. Hence, the model was highly adaptable in the prediction of the degradation efficiency by varying the variables in the studied range.

Table 3 reports the ANOVA results for the experimental data collected from the study of RSM. The CCD model was statistically significant due to the *F*-value of 89.13

Table 2
Designed matrix according to CCD method alongwith the predicted and experimental degradation efficiency of MG dye

Run order	Catalyst loading (g/L)	Initial dye concentration (mg/L)	Ultrasonic power (W)	Oxidant concentration (mM)	Degradation efficiency (%)	
					Actual value	Predicted value
1	0.75	1,250	40	1.75	53.14	52.52
2	0.75	500	80	1.75	86.16	79.67
3	0.75	1,250	40	0.75	28.24	31.28
4	1.5	500	40	1.75	89.49	91.66
5	0.75	1,250	80	1.75	51.68	58.28
6	1.125	875	60	0.25	41.21	40.23
7	0.375	875	60	1.25	59.46	55.25
8	0.75	500	40	1.75	88.33	85.43
9	1.125	875	60	2.25	82.52	82.71
10	0.75	500	80	0.75	58.46	58.44
11	1.5	1,250	40	1.75	56.21	58.74
12	1.125	875	60	1.25	59.95	61.47
13	1.125	125	60	1.25	86.04	88.63
14	1.5	1,250	80	1.75	70.44	64.50
15	1.5	500	80	1.75	88.21	85.90
16	1.125	875	20	1.25	56.58	61.47
17	1.125	875	60	1.25	65	61.47
18	1.5	500	40	0.75	69.71	70.42
19	0.75	500	40	0.75	59.81	64.20
20	1.125	875	60	1.25	50.38	61.47
21	1.125	875	60	1.25	61.8	61.47
22	1.5	1,250	40	0.75	37.64	37.50
23	0.75	1,250	80	0.75	37.47	37.04
24	1.875	875	60	1.25	62.54	67.69
25	1.5	500	80	0.75	66.45	64.66
26	1.125	875	60	1.25	65.19	61.47
27	1.125	1,625	60	1.25	32.17	34.31
28	1.125	875	60	1.25	64.02	61.47
29	1.125	875	100	1.25	62.1	61.47
30	1.5	1,250	80	0.75	53.66	43.26

corresponding with the p-value < 0.0001. The results indicated that there was only a 0.01% chance that the F-value could occur due to noise. In addition, the model with a small lack of fit F-value of 0.5860 implied that the model mismatch was insignificant. There was an 82.08% chance that a lack of fit F-value could occur due to noise. The adequate precision of this model was evaluated at a value 32.2527 which was larger than 4, indicated the adequacy of the model in the prediction of experimental response with a high ratio of signal to noise. In this case, A, B, D and BC were the significant model terms with p-values smaller than 0.05.

3.3.1. Effect of experimental variables on the degradation efficiency

Fig. 7a represents the effect of catalyst loading and initial dye concentration on the degradation efficiency of MG at constant ultrasonic power of 60 W and oxidant concentration of 1.25 mM. The 3D surface plot shows that the degradation efficiency of MG increased slightly with the increasing catalyst loading. This was owing to the increment in the electron–hole pair leading to the generation of more active oxidizing species such as hydroxyl and sulphate radicals [36]. In addition, a greater amount of catalyst loading increased the surface area available for the adsorption of pollutants and hence improved the degradation efficiency [37]. However, the sonocatalytic degradation efficiency was quenched by the increasing initial dye concentration. This was attributed to the less effective heat and energy absorption with the increasing amount of dye molecules adsorbed on the catalyst surface [27]. Hence, the better degradation efficiency of MG can be attained at higher catalyst loading and lower initial dye concentration.

Fig. 7b illustrates the effect of catalyst loading and ultrasonic power on the sonocatalytic degradation efficiency at a constant oxidant concentration of 1.25 mM and initial dye concentration of 875 mg/L. The findings showed that the degradation efficiency of MG dye increased slightly

with increasing catalyst loading and ultrasonic power. According to Xu et al. [34], an increment in the ultrasonic power resulted in strengthened acoustic power and higher acoustic amplitude. This led to the formation of more microbubbles in the aqueous reacting medium with higher potential energy. Accompanied by the increasing catalyst loading, the generation of acoustic bubbles was further enhanced due to more nucleation sites present in the system [38]. As a consequence, the formation of electron–hole pair on the surface of sonocatalyst was facilitated and a higher amount of ROS was generated due to the higher photon energy induced by higher ultrasonic power. In addition, the microjet speed of cavitation bubbles was generated in the liquid medium with higher ultrasonic power leading to the improvement in the mass transfer rate of reactants and products. The continuously cleaning effect applied on the surface of sonocatalyst by the ultrasound wave was also enhanced by increasing the ultrasonic power [35]. The total surface active sites for the possible reactions could also be increased by increasing the catalyst loading [3]. Therefore, more adsorption of MG molecules onto the sonocatalyst prior to the degradation into final products. This led to the improvement of sonocatalytic MG degradation efficiency.

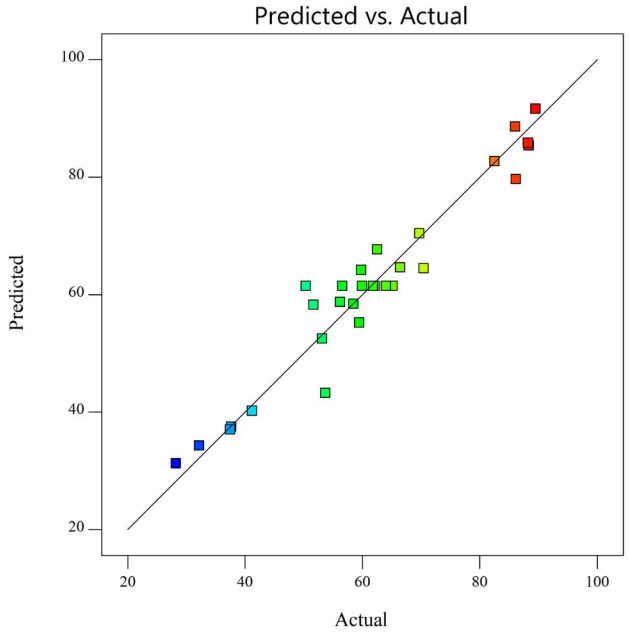

Fig. 6. The relationship between predicted and experimental data of sonocatalytic degradation efficiency.

Fig. 7c shows a three-dimensional surface plot representing the interactive effect of catalyst loading and oxidant concentration on the response of sonocatalytic degradation efficiency at a constant initial dye concentration of 875 mg/L and ultrasonic power of 60 W. It was found that there was an increasing trend on the degradation efficiency of MG dye with both the increasing catalyst loading and oxidant concentration. As the activation of persulfate ions was performed through an electron transfer mechanism as presented in Eq. (4), a higher catalyst loading provided a bigger surface area of the active site and more electron for the activation of persulfate ions [39]. A higher amount of catalyst loading also led to the production of more radicals from water and oxygen molecules under ultrasound irradiation. In this case, oxidant concentration had a greater positive effect than catalyst loading on the outcome of degradation efficiency. This was because a higher amount of sodium persulfate present in the degradation could produce a greater amount of persulfate ions. In addition, a greater amount of persulfate ions increased the lifetime of electron-hole pairs formed on the surface of the catalyst by inhibiting their recombination rate [18]. This was able to improve the degradation efficiency of MG dye to an appreciable extent by the greater amount of reactive radicals with strong oxidizing power. Therefore, the designed model revealed that the sonocatalytic dye decomposition could be improved by the combination of high catalyst loading and high oxidant concentration.

Fig. 7d presents the influence of initial dye concentration and ultrasonic power at a constant catalyst loading of 1.125 g/L and oxidant concentration of 1.25 mM. These two parameters showed a significant interactive effect on the degradation efficiency of MG dye with a p-value of 0.0113. The findings depicted that the degradation efficiency of MG decreased with increasing initial dye concentration. This was due to the limited number of radicals available for dye degradation at higher initial dye concentrations [2].

Table 3
ANOVA results for sonocatalytic degradation efficiency of MG dye

Source	Sum of squares	Freedom degrees	Mean square	F-value	p-value	
Model	7,495.97	4	1,873.99	89.13	<0.0001	Significant
A-Catalyst loading	232.38	1	232.38	11.05	0.0027	
B-Initial dye concentration	4,424.91	1	4,424.91	210.45	<0.0001	
D-Oxidant concentration	2,705.98	1	2,705.98	128.70	<0.0001	
BC	132.71	1	132.71	6.31	0.0188	
Residual	525.65	25	21.03			
Lack of fit	368.47	20	18.42	0.5860	0.8208	Not significant
Pure error	157.18	5	31.44			
Cor. total	8,021.62	29				
R^2 = 0.9345; Adequate precision = 32.2527						

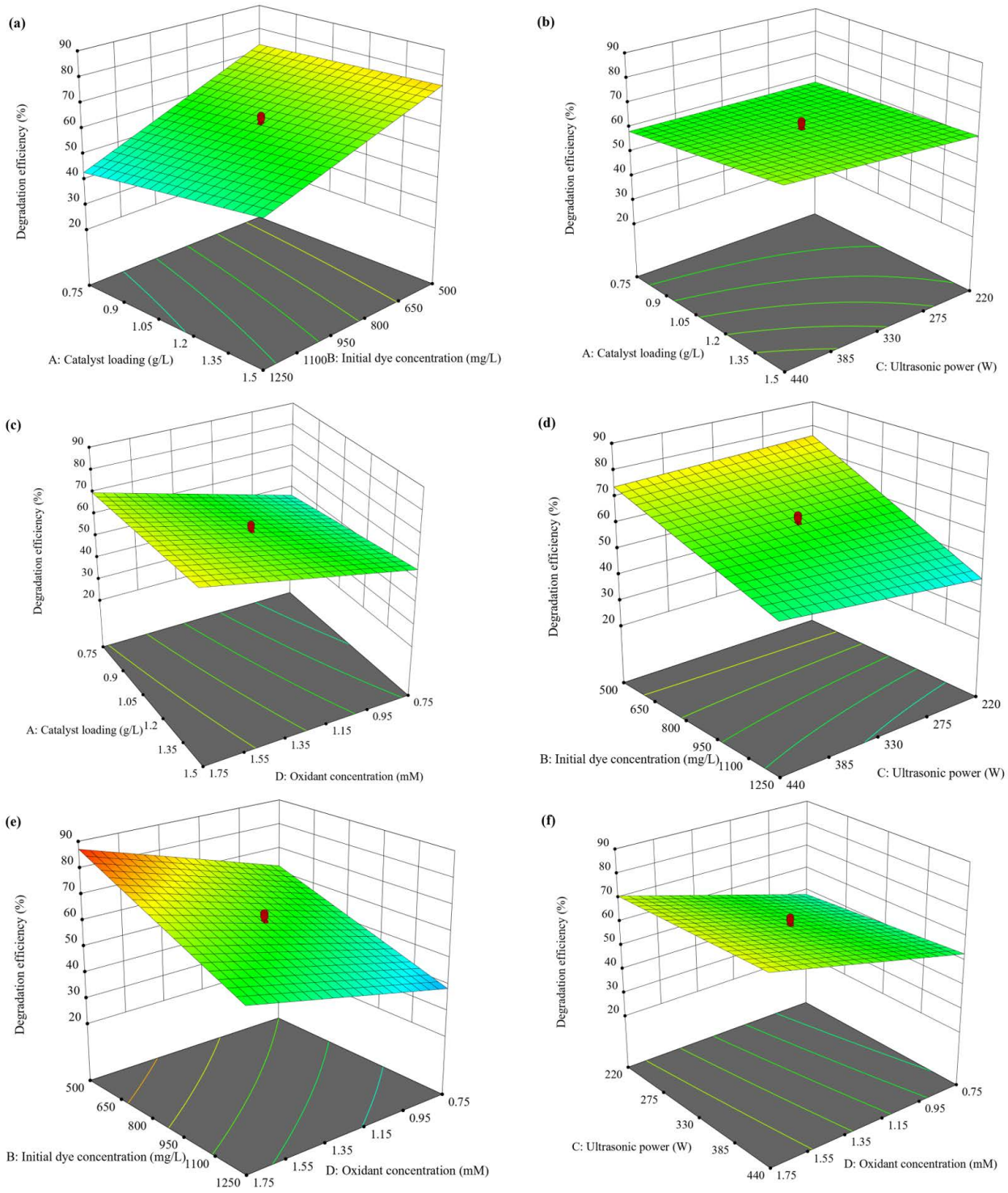

Fig. 7. Interactive effects of (a) catalyst loading and initial dye concentration, (b) catalyst loading and ultrasonic power, (c) catalyst loading and oxidant concentration, (d) initial dye concentration and ultrasonic power, (e) initial dye concentration and oxidant concentration and (f) ultrasonic power and oxidant concentration.

From this point of view, the performance of the sonocatalytic decomposition could be enhanced by increasing the ultrasonic power because the shock wave with higher intensity could be induced under greater ultrasonic power condition leading to more generation of active oxidizing species [27]. Therefore, the degradation of MG could be enhanced by increasing the ultrasonic power and decreasing initial dye concentration.

Fig. 7e shows the effect of oxidant concentration and initial dye concentration on the performance of sonocatalytic degradation at a constant catalyst loading of 1.125 g/L and ultrasonic power of 60 W. According to the results of the study, the degradation efficiency of MG is inversely correlated to the initial dye concentration. As discussed by Chu et al. [39], the adsorption of dye molecules on the catalyst surface might decrease the surface area available for the generation of radicals at higher initial dye concentration. Anyhow, the degradation efficiency of MG could be improved at higher oxidant concentrations due to the greater amount of radicals available to decompose the organic dye compounds [2]. Hence, the combination of lower initial dye concentration and higher oxidant concentration could improve the performance of sonocatalytic degradation.

Fig. 7f depicts the interactive effect of oxidant concentration and ultrasonic power on the degradation efficiency at a constant catalyst loading of 1.125 g/L and initial dye concentration of 875 mg/L. According to Fig. 7f, the highest degradation efficiency could be achieved by maximizing both the oxidant concentration and ultrasonic power. This was because the persulfate ions could be activated directly under ultrasonic irradiation to form sulphate radicals. The generated sulphate radicals triggered the yield of other radicals by breaking down the water molecules into hydroxyl radicals and hence resulted in the oxidation of organic dye [40]. The sound wave intensity increased with increasing ultrasonic power. This brought to the increment in the energy and quality of bubble cavitation which induced high pressure gradient in the liquid medium [41]. As a result, more conversion of persulfate ions could occur which enhanced the yield radicals. Eventually, the degradation efficiency of MG dye was improved with the increasing oxidant concentration under high ultrasonic power.

3.3.2. Optimization of degradation efficiency

According to the results obtained from the RSM modelling, the maximum degradation efficiency of MG dye was able to be determined through the optimization of the studied experimental variables. Fig. 8 presents the change of UV-Vis spectra of MG dye under the optimum condition of sonocatalytic degradation. The predicted degradation efficiency was 90.03% which was evaluated using Eq. (4). The actual optimum degradation efficiency of MG dye obtained through the experiment was 89.21%. The experimental value of degradation efficiency exhibited a negligible error percentage of 0.91% with the predicted value. The results again proved that the model could be applied convincingly in the prediction and optimization of MG dye degradation efficiency.

As shown in Fig. 8, the presence of acid function of oxalate species, aromatic rings and chromophore in the MG dye was confirmed by the characterization peaks at 316, 425 and 617 nm [42]. It is noteworthy that the maximum absorbance peak at 617 nm showed a dramatic decrease implying that the structure of chromophore was destroyed which resulted in the nearly invisible solution after undergoing the sonocatalytic degradation [43]. Besides, a decreasing trend was observed at the peaks with wavelengths of 316 and 425 nm which was owing to the cleavage of central

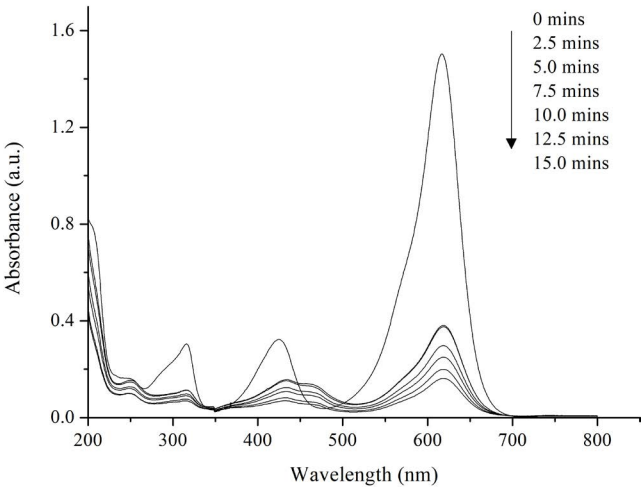

Fig. 8. Sonocatalytic degradation of MG under the optimized condition. (Initial dye concentration = 500 mg/L, catalyst loading = 0.75 g/L, concentration of oxidant = 1.75 mM, ultrasonic power = 40 W).

carbon and breakage of aromatic rings [44]. In addition, the new peak observed at 251 nm was owing to the formation of single-benzene derivatives during the degradation of MG molecules [45]. Both the decrements of MG original peaks and the presence of new peaks indicated that MG compounds were degraded during the sonocatalytic process. The findings were in good agreement with Yulizar et al. [46] which observed the photocatalytic degradation of MG using a UV-Vis spectrophotometer.

The COD removal efficiency was found to be 59.37% after 15 min of sonocatalytic degradation process under the optimum operating condition. The decrease in COD value showed the decomposition of MG molecules in the presence of Ag-ZnO as catalyst and sodium persulfate as oxidant under ultrasound irradiation. The remaining COD was contributed by the metabolites generated during the degradation of MG compounds as identified in the previous paragraph.

Fig. 9 shows the FTIR spectra of MG molecules, fresh Ag-ZnO and used Ag-ZnO nanoparticles. The FTIR spectrum of MG exhibited characteristic peaks at 1,577; 1,153 and 2,900 cm^{-1} corresponding to the C=C stretching of benzene rings, C–N stretching vibration of the amino group and C–H stretching of asymmetric CH_3 group respectively. The peaks appeared in the range of 850 and 670 cm^{-1} were assigned to the aromatic structure present in MG molecules [47]. By comparing to the FTIR spectrum of fresh Ag-ZnO, there was no change in the chemical structure of Ag-ZnO after undergoing sonocatalytic degradation of MG dye. The broad peaks present at 3,378 and 1,600 cm^{-1} in the spectrum of used Ag-ZnO were due to the stretching vibration and deformation vibration of hydroxyl groups respectively, implying moisture content on the nanoparticles [48]. Besides, it is noteworthy that there was no fingerprint of MG found in the spectrum of used Ag-ZnO. The findings concluded that the decrements in the concentration of MG solutions were attributed to the decomposition reaction instead of adsorption on the Ag-ZnO nanoparticles.

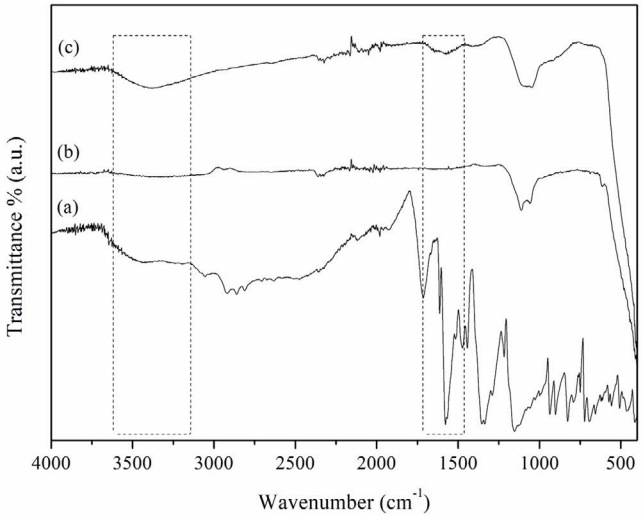

Fig. 9. FTIR spectra of (a) MG, (b) fresh Ag-ZnO and (c) spent Ag-ZnO.

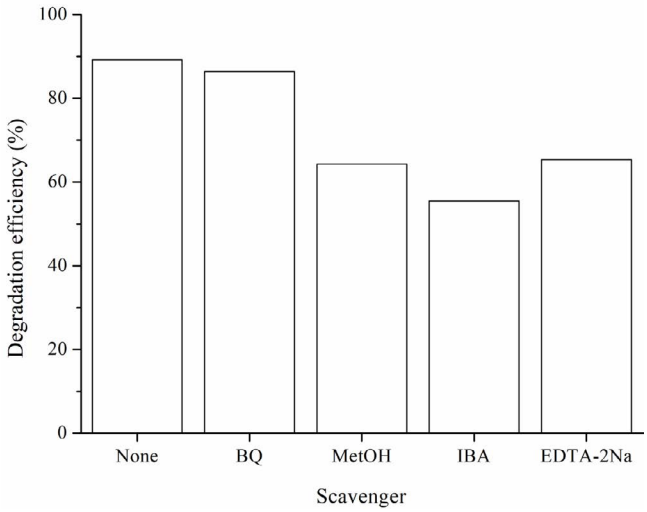

Fig. 10. Effect of chemical scavengers on the degradation of MG dye in the presence of Ag-ZnO as catalyst and sodium persulfate as oxidant under ultrasonic irradiation.

Fig. 10 illustrates the effect of scavenger addition on the sonocatalytic degradation efficiency of MG dye. It is noteworthy that the degradation efficiencies of MG dye were quenched from 89.21% to 86.41%, 64.27%, 55.47% and 65.33% in the presence of BQ, MetOH, IBA and $K_2Cr_2O_7$ respectively. The results obtained from the radical scavenging study confirmed the presence of superoxide radicals, hydroxyl radicals, sulphate radicals and holes in the sonocatalytic degradation of MG dye. The findings also revealed that hydroxyl radical was the dominant active species in the sonocatalytic oxidation of MG dye as the degradation efficiency was suppressed the most in the presence of IBA. Lv et al. [49] reported similar results indicating that hydroxyl radical was an important oxidizing species involved in the degradation of organic compounds through the AOPs.

Table 4 compares the current finding of ultrasound-assisted removal of MG with the literatures. The comparison revealed that the amount of MG degraded under optimum condition in current work was the greatest among the reported works with the lowest energy consumption and shortest reaction time. This remarks the feasibility of green synthesis to produce Ag-ZnO nanoparticles as one of the potential candidates to be used as a sonocatalyst in the degradation of organic dye.

3.4. Reusability study

Fig. 11a illustrates the XRD spectra of fresh and spent Ag-ZnO. The characteristic peaks observed in the spectra verified the hexagonal wurtzite phase of ZnO as identified

Table 4
Comparative data on the degradation of MG

Removal technique	Energy source	Catalyst	Catalyst dosage (g/L)	Dye concentration (mg/L)	Reaction time (min)	Degradation efficiency (%)	Reference
Sonocatalysis	40 W ultrasound	Ag-ZnO	0.75	500	15	89.21	Present work
Sonocatalysis	300 W ultrasound	$NiGa_2O_4/CeO_2$	1.0	10	60	96.2	[56]
Sonocatalysis	–	Zeolite imidazole framework-8	0.05	25	90	95.0	[57]
Ultrasonic-electrochemical	300 W ultrasound	Ruthernium-iridium plated titanium electrode	–	100	60	94.92	[58]
Sonophotocatalysis	127 W ultrasound	Chitosan-Ascorbic Acid@$NiFe_2O_4$ Spinel Ferrite	1.0	70	90	99.05	[59]
Sono-assisted adsorption	–	Magnesium ferrite	0.5	50	15	90.0	[60]

in JCPDS card no: 36-1451 [50]. The diffraction peaks of ZnO observed at 2θ = 31.8°, 34.4°, 36.3°, 47.6°, 56.6°, 62.9°, 66.4°, 68.0° and 69.1° were owing to the planes (100), (002), (101), (102), (110), (103), (200), (112) and (201), respectively [51]. Besides, the presence of face-centered cubic Ag in Ag-ZnO was confirmed according to the peaks observed at 2θ = 38.1°, 44.3°, 64.4° and 77.3° were attributed to the planes (111), (200), (220) and (311). The characteristic peaks of metallic Ag was found to be in line with JCPDS card no: 04-0783 [52]. Fig. 11a reveals that there was no change in the characteristic peaks of Ag-ZnO. The findings implied the crystallites of Ag-ZnO was hardly affected by the shockwave produced during the collapse of cavities. Fig. 11b shows the sonocatalytic degradation efficiency of MG in the presence of fresh and reused catalyst up to five catalytic cycles. The result of the first catalytic cycle was obtained by using the fresh Ag-ZnO as sonocatalyst. As presented in Fig. 11b, the degradation efficiency merely decreased by 10% in the 5th catalytic cycle of the sonocatalysis process. The high stability of Ag-ZnO reflected the feasibility of the green synthesized ZnO nanoparticles to be used as sonocatalyst in commercial application.

3.5. Mechanism of sonocatalysis

The degradation of organic dye under ultrasound irradiation can be divided into two main processes which are sonolysis and sonocatalysis. In sonolysis process, the acoustic cavitation effect occurs including the formation, growth and collapse of microbubbles in the aqueous solution. Basically, the cavitation nuclei of bubbles are originated from the gas molecules or vapor which fill up the void space of liquid [53]. The bubbles will then expand into bigger size and eventually implode. The collapse of bubbles lead to the generation of hotspot with critical pressure of 1,000 atm and temperature of 5,000 K [2]. This results in the pyrolysis of water and oxygen molecules into hydroxyl, superoxide and hydrogen radicals as illustrated in Eqs. (5)–(7) [35]:

$$H_2O \rightarrow {}^{\bullet}OH + {}^{\bullet}H \quad (5)$$

$$O_2 \rightarrow 2{}^{\bullet}O \quad (6)$$

$${}^{\bullet}O + H_2O \rightarrow 2{}^{\bullet}OH \quad (7)$$

In the sonocatalysis process, the presence of heterogeneous catalyst can enhance the formation of radicals by providing more nucleation sites for the acoustic bubbles [4]. Besides, photons irradiation can be induced in the sonicated solution in the form of sonoluminescence which is able to excite surface electron of nanoparticles from the valence band to the conduction band [33]. The separation ability of electron-hole pair and the lifetime of charge carriers are the important factors that affect the sonocatalytic degradation efficiency [54]. The formation of the charge carriers followed by the conversion of the water and oxygen molecules into various types of radical as presented in the following equations [34]:

$$\text{Sonocatalyst} + \text{Sonoluminescence} \rightarrow e^- + h^+ \quad (8)$$

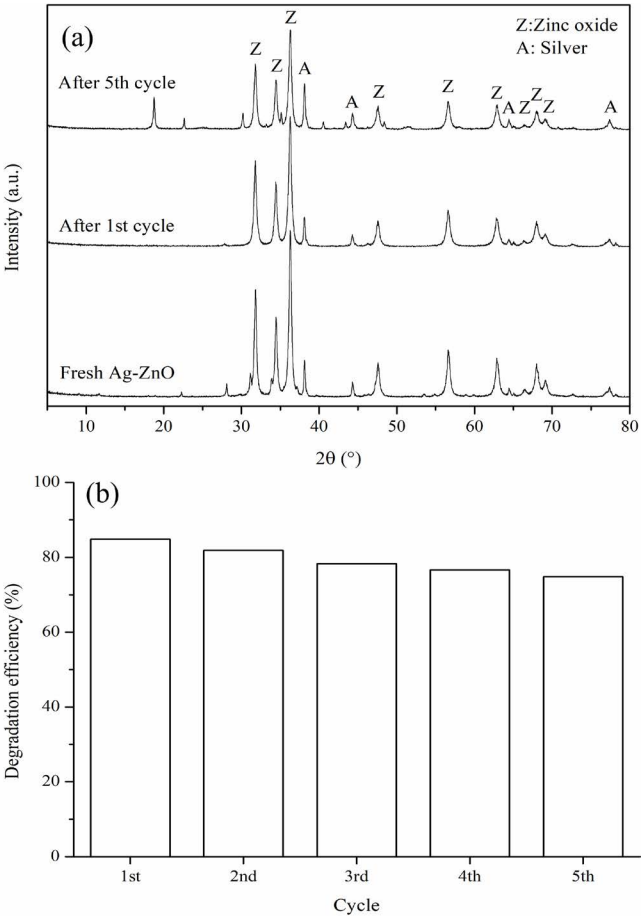

Fig. 11. (a) XRD spectra of fresh and spent Ag-ZnO and (b) reusability test of Ag-ZnO in term of the sonocatalytic performance in the degradation of MG.

$$H_2O + h^+ \rightarrow {}^{\bullet}OH + H^+ \quad (9)$$

$$O_2 + e^- \rightarrow {}^{\bullet}O_2^- \quad (10)$$

$${}^{\bullet}O_2^- + H^+ \rightarrow {}^{\bullet}OOH \quad (11)$$

$$2{}^{\bullet}OOH \rightarrow H_2O_2 + O_2 \quad (12)$$

$$H_2O_2 + {}^{\bullet}O_2^- \rightarrow {}^{\bullet}OH + OH^- + O_2 \quad (13)$$

Accompanied with the Ag doping, the sonocatalytic degradation efficiency of MG in the presence of ZnO nanoparticles was improved due to the prolonged lifetime of charge carriers as confirmed through PL analysis. The transition of excited electron would occur favourably from the valence band of ZnO nanoparticles to the metallic Ag rather than conduction band of ZnO. This was owing to the lower level of Fermi energy of Ag-ZnO than the conduction band of ZnO [55]. Therefore, the presence of metallic Ag as electron trap resulted in better separation efficiency of electron–hole pair which would enhance the generation of free radicals for dye degradation. In addition,

thermocatalytic process can also be resulted from the acoustic cavitation during ultrasonic irradiation. Pyrolysis of water molecules and formation of electron–hole pair of catalyst can be further enhanced by thermal energy resulted from the immense local temperature of bubble collapse [27].

The presence of persulfate can improve the generation of free radicals through self-decomposition and water pyrolysis under ultrasound irradiation as shown in Eqs. (14) and (15) respectively [2]:

$$S_2O_8^{2-} \rightarrow 2SO_4^{\bullet-} \quad (14)$$

$$SO_4^{\bullet-} + H_2O \rightarrow {}^{\bullet}OH + SO_4^{\bullet-} + H^+ \quad (15)$$

All these free radicals generated eventually play significant roles in the degradation of organic dye. The results of radical scavenging test displayed in Fig. 10 supported the role of radicals in the decomposition of organic dye. According to the UV-Vis spectra presented in Fig. 8, the free radicals with high oxidizing power will attack the central carbon and break the aromatic rings. In addition, the mechanism will also be extended to the breakage of C=C and C=N bonds of chromophore, leading to the decolourization of organic dye. In the final stage of sonocatalytic degradation, the organic pollutant will be degraded into carbon dioxide and water molecules ideally.

3.6. Advantages and limitations

The main advantage of this study includes the usage of *Clitoria ternatea* Linn plant as green material in the production of ZnO nanoparticles instead of the hazardous chemicals such as sodium hydroxide and ammonia solution. The findings revealed the potential of green synthesis to be applied as an alternative in the commercial due to its environmentally friendly feature. Besides, the application of sonocatalysis in this work is fitted well to the principles of green chemistry, which is a heterogeneous catalysis designed for the degradation of organic pollutant under milder conditions with low energy consumption. This research also employed RSM in the optimization of sonocatalysis process which achieved the time and labour saving as compared to one-factor-at-a-time method. However, several suggestions are provided for future work investigation to overcome the limitations observed in this study such as modification of Ag-ZnO based on the consideration of ease for recovery issue as well as the necessity of the pilot-scale testing prior to the application in industry.

4. Conclusions

The size reduction of ZnO nanoparticles was able to be achieved through the green synthesis process using *Clitoria ternatea* Linn extract. Besides, the sonocatalytic performance of ZnO powder in the degradation of MG dye was able to be enhanced by the incorporation of Ag as a dopant into the matrix of ZnO. A modified second-order equation was obtained through the RSM to evaluate the sonocatalytic degradation efficiency of MG dye. The ANOVA results indicated that the constructed central composite model which was statistically significant with p-value < 0.0001 could predict sonocatalytic degradation efficiency with high accuracy in the studied range of experimental variables. This model exhibited high adequacy of 32.2527 and a high coefficient of determination of 0.9345. The optimum degradation efficiency of MG dye was found to be 89.21% after 15 min under the condition with 0.75 g/L of Ag-ZnO as a catalyst, 500 mg/L of initial dye concentration and 1.75 mM of sodium persulfate as oxidant and 40 W of power to generate ultrasound irradiation. The radical scavenging test confirmed the involvement of superoxide radicals, hydroxyl radicals, sulphate radicals and holes in the sonocatalytic degradation of MG dye.

Acknowledgements

The authors gratefully acknowledge gratefully the Fundamental Research Grant Scheme (FRGS/1/2018/TK10/UTAR/02/2) by the Ministry of Education (MOE) Malaysia, the Universiti Tunku Abdul Rahman (UTAR) Research Fund (UTARRF/2020-C2/P01) and Kurita Water and Environment Foundation (KWEF) that provided the Kurita Overseas Research Grant (21Pmy076) for the financial support on this project.

References

[1] World Health Organization, Drinking-Water, 2019. Available at: https://www.who.int/news-room/fact-sheets/detail/drinking-water
[2] S. Ahmadi, A. Rahdar, C. Adaobi Igwegbe, S. Mortazavi-Derazkola, A. Marek Banach, S. Rahdar, A. Kumar Singh, S. Rodriguez-Couto, G.Z. Kyzas, Praseodymium-doped cadmium tungstate ($CdWO_4$) nanoparticles for dye degradation with sonocatalytic process, Polyhedron, 190 (2020) 114792, doi: 10.1016/j.poly.2020.114792.
[3] O.S. Ayanda, O.H. Aremu, C.O. Akintayo, K.O. Sodeinde, W.N. Igboama, E.O. Oseghe, S.M. Nelana, Sonocatalytic degradation of amoxicillin from aquaculture effluent by zinc oxide nanoparticles, Environ. Nanotechnol. Monit. Manage., 16 (2021) 100513, doi: 10.1016/j.enmm.2021.100513.
[4] L.-L. He, Y. Zhu, Q. Qi, X.-Y. Li, J.-Y. Bai, Z. Xiang, X. Wang, Synthesis of $CaMoO_4$ microspheres with enhanced sonocatalytic performance for the removal of Acid Orange 7 in the aqueous environment, Sep. Purif. Technol., 276 (2021) 119370, doi: 10.1016/j.seppur.2021.119370.
[5] R. Anugrahwidya, N. Yudasari, D. Tahir, Optical and structural investigation of synthesis ZnO/Ag nanoparticles prepared by laser ablation in liquid, Mater. Sci. Semicond. Process., 105 (2020) 104712, doi: 10.1016/j.mssp.2019.104712.
[6] V.V. Kadam, S.D. Shanmugam, J.P. Ettiyappan, R.M. Balakrishnan, Photocatalytic degradation of p-nitrophenol using biologically synthesized ZnO nanoparticles, Environ. Sci. Pollut. Res. Int., 28 (2021) 12119–12130.
[7] N. Venkatesh, S. Aravindan, K. Ramki, G. Murugadoss, R. Thangamuthu, P. Sakthivel, Sunlight-driven enhanced photocatalytic activity of bandgap narrowing Sn-doped ZnO nanoparticles, Environ. Sci. Pollut. Res., 28 (2021) 16792–16803.
[8] Ch Venkata Reddy, I. Neelakanta Reddy, V.V.N. Harish, K.R. Reddy, N.P. Shetti, J. Shim, T.M. Aminabhavi, Efficient removal of toxic organic dyes and photoelectrochemical properties of iron-doped zirconia nanoparticles, Chemosphere, 239 (2020) 124766, doi: 10.1016/j.chemosphere.2019.124766.
[9] D. Kwon, J. Kim, Silver-doped ZnO for photocatalytic degradation of methylene blue, Korean J. Chem. Eng., 37 (2020) 1226–1232.
[10] M. Özcan, B. Birol, F. Kaya, Investigation of photocatalytic properties of TiO_2 nanoparticle coating on fly ash and red

mud based porous ceramic substrate, Ceram. Int., 47 (2021) 24270–24280.
[11] M. Bandeira, M. Giovanela, M. Roesch-Ely, D.M. Devine, J. da Silva Crespo, Green synthesis of zinc oxide nanoparticles: a review of the synthesis methodology and mechanism of formation, Sustainable Chem. Pharm., 15 (2020) 100223, doi: 10.1016/j.scp.2020.100223.
[12] G.A. Molina, R. Esparza, J. Luis López-Miranda, A.R. Hernández-Martínez, B.L. España-Sánchez, E.A. Elizalde-Peña, M. Estevez, Green synthesis of Ag nanoflowers using Kalanchoe Daigremontiana extract for enhanced photocatalytic and antibacterial activities, Colloids Surf., B, 180 (2019) 141–149.
[13] A. Jayakumar, R.K. Vedhaiyan, Rapid synthesis of phytogenic silver nanoparticles using *Clerodendrum splendens*: its antibacterial and antioxidant activities, Korean J. Chem. Eng., 36 (2019) 1869–1881.
[14] J.L. Luna-Sánchez, J.L. Jiménez-Pérez, R. Carbajal-Valdez, G. Lopez-Gamboa, M. Pérez-González, Z.N. Correa-Pacheco, Green synthesis of silver nanoparticles using Jalapeño Chili extract and thermal lens study of acrylic resin nanocomposites, Thermochim. Acta, 678 (2019) 178314, doi: 10.1016/j.tca.2019.178314.
[15] B. Thomas, B. Scholastica Mary Vithiya, T. Augustine Arul Prasad, S.B. Mohamed, C. Maria Magdalane, K. Kaviyarasu, M. Maaza, Antioxidant and photocatalytic activity of aqueous leaf extract mediated green synthesis of silver nanoparticles using *Passiflora edulis f. flavicarpa*, Mater. Today:. Proc., 14 (2019) 239–247.
[16] B. Kaur, L. Kuntus, P. Tikker, E. Kattel, M. Trapido, N. Dulova, Photo-induced oxidation of ceftriaxone by persulfate in the presence of iron oxides, Sci. Total Environ., 676 (2019) 165–175.
[17] M. Sabri, A. Habibi-Yangjeh, S. Vadivel, Novel ZnO/$Ag_6Si_2O_7$ nanocomposites for activation of persulfate ions in photocatalytic removal of organic contaminants under visible light, Mater. Chem. Phys., 239 (2020) 121988, doi: 10.1016/j.matchemphys.2019.121988.
[18] G.B. Jegadeesan, S. Amirthavarshini, J. Divya, G.I. Gunarani, Catalytic peroxygen activation by biosynthesized iron nanoparticles for enhanced degradation of Congo red dye, Adv. Powder Technol., 30 (2019) 2890–2899.
[19] G.B. Escher, M.B. Marques, M.A.V. do Carmo, L. Azevedo, M.M. Furtado, A.S. Sant'Ana, M.C. da Silva, M.I. Genovese, M. Wen, L. Zhang, W.Y. Oh, F. Shahidi, N.D. Rosso, D. Granato, *Clitoria ternatea* L. petal bioactive compounds display antioxidant, antihemolytic and antihypertensive effects, inhibit α-amylase and α-glucosidase activities and reduce human LDL cholesterol and DNA induced oxidation, Food Res. Int., 128 (2020) 108763, doi: 10.1016/j.foodres.2019.108763.
[20] M. Zulfiqar, S. Chowdhury, A.A. Omar, A.A. Siyal, S. Sufian, Response surface methodology and artificial neural network for remediation of acid orange 7 using TiO_2-P25: optimization and modeling approach, Environ. Sci. Pollut. Res., 27 (2020) 34018–34036.
[21] S.M. Tabrizi Hafez Moghaddas, B. Elahi, M. Darroudi, V. Javanbakht, Green synthesis of hexagonal-shaped zinc oxide nanosheets using mucilage from flaxseed for removal of methylene blue from aqueous solution, J. Mol. Liq., 296 (2019) 111834, doi: 10.1016/j.molliq.2019.111834.
[22] O.T. Jemilugba, E.H.M. Sakho, S. Parani, V. Mavumengwana, O.S. Oluwafemi, Green synthesis of silver nanoparticles using *Combretum erythrophyllum* leaves and its antibacterial activities, Colloid Interface Sci. Commun., 31 (2019) 100191, doi: 10.1016/j.colcom.2019.100191.
[23] K. Rambabu, G. Bharath, F. Banat, P.L. Show, Green synthesis of zinc oxide nanoparticles using *Phoenix dactylifera* waste as bioreductant for effective dye degradation and antibacterial performance in wastewater treatment, J. Hazard. Mater., 402 (2021) 123560, doi: 10.1016/j.jhazmat.2020.123560.
[24] N. Pauzi, N.M. Zain, N.A.A. Yusof, Gum arabic as natural stabilizing agent in green synthesis of ZnO nanofluids for antibacterial application, J. Environ. Chem. Eng., 8 (2019) 103331, doi: 10.1016/j.jece.2019.103331.
[25] Sukriti, P. Chand, V. Singh, Enhanced visible-light photocatalytic activity of samarium-doped zinc oxide nanostructures, J. Rare Earths, 38 (2019) 29–38.
[26] A. Chinnathambi, Synthesis and characterization of spinel FeV_2O_4 coupled ZnO nanoplates for boosted white light photocatalysis and antibacterial applications, J. Alloys Compd., 890 (2022) 161742, doi: 10.1016/j.jallcom.2021.161742.
[27] A. Mehrizad, M.A. Behnajady, P. Gharbani, S. Sabbagh, Sonocatalytic degradation of Acid Red 1 by sonochemically synthesized zinc sulfide-titanium dioxide nanotubes: optimization, kinetics and thermodynamics studies, J. Cleaner Prod., 215 (2019) 1341–1350.
[28] R. Jothi Ramalingam, T. Radhika, P. Reshma Ranjan, S.R.M. Sayed, H.A. Al-Lohedan, A. Meera Moydeen, D.M. Al-dhayan, Platinum nanoparticle decorated rutile titania synthesized by surfactant free hydrothermal method for visible light catalysis for dye degradation and hydrogen production study, Int. J. Hydrogen Energy, 44 (2019) 23959–23968.
[29] A. Moosavi, A.A. Amooey, A.A. Mir, M.H. Marzbali, Extraordinary adsorption of acidic fuchsine and malachite green onto cheap nano-adsorbent derived from eggshell, Chin. J. Chem. Eng., 28 (2020) 1591–1602.
[30] A.A. Ahmad, M.A. Ahmad, N.K.E.M. Yahaya, J. Karim, Adsorption of malachite green by activated carbon derived from gasified *Hevea brasiliensis* root, Arabian J. Chem., 14 (2021) 103104, doi: 10.1016/j.arabjc.2021.103104.
[31] S. Munyai, Z.N. Tetana, M.M. Mathipa, B. Ntsendwana, N.C. Hintsho-Mbita, Green synthesis of cadmium sulphide nanoparticles for the photodegradation of malachite green dye, sulfisoxazole and removal of bacteria, Optik (Stuttg), 247 (2021) 167851, doi: 10.1016/j.ijleo.2021.167851.
[32] Y.Y. Chan, Y.L. Pang, S. Lim, C.W. Lai, A.Z. Abdullah, W.C. Chong, Biosynthesized Fe- and Ag-doped ZnO nanoparticles using aqueous extract of *Clitoria ternatea* Linn for enhancement of sonocatalytic degradation of Congo red, Environ. Sci. Pollut. Res., 27 (2020) 34675–34691.
[33] P. Sravandas, L.K. Alexander, Facile hydrothermal synthesis and sonophotocatalytic performance of novel Bi_2WO_6 structure on the degradation of rhodamine B, Mater. Today:. Proc., 46 (2021) 2925–2929.
[34] L. Xu, X. Wang, M.-L. Xu, B. Liu, X.-F. Wang, S.-H. Wang, T. Sun, Preparation of zinc tungstate nanomaterial and its sonocatalytic degradation of meloxicam as a novel sonocatalyst in aqueous solution, Ultrason. Sonochem., 61 (2019) 104815, doi: 10.1016/j.ultsonch.2019.104815.
[35] A.F. Hassan, H. Elhadidy, Effect of Zr^{+4} doping on characteristics and sonocatalytic activity of TiO_2/carbon nanotubes composite catalyst for degradation of chlorpyrifos, J. Phys. Chem. Solids, 129 (2019) 180–187.
[36] Á. de J. Ruíz-Baltazar, Sonochemical activation-assisted biosynthesis of Au/Fe_3O_4 nanoparticles and sonocatalytic degradation of methyl orange, Ultrason. Sonochem., 73 (2021) 105521, doi: 10.1016/j.ultsonch.2021.105521.
[37] B. Rahimi, N. Jafari, A. Abdolahnejad, H. Farrokhzadeh, A. Ebrahimi, Application of efficient photocatalytic process using a novel BiVO/TiO_2-NaY zeolite composite for removal of acid orange 10 dye in aqueous solutions: modeling by response surface methodology (RSM), J. Environ. Chem. Eng., 7 (2019) 103253, doi: 10.1016/j.jece.2019.103253.
[38] G.K. Dinesh, S. Chakma, Degradation kinetic study of cholesterol lowering statin drug using sono-hybrid techniques initiated by metal-free polymeric catalyst, J. Taiwan Inst. Chem. Eng., 100 (2019) 95–104.
[39] J.-H. Chu, J.-K. Kang, S.-J. Park, C.-G. Lee, Enhanced sonocatalytic degradation of bisphenol A with a magnetically recoverable biochar composite using rice husk and rice bran as substrate, J. Environ. Chem. Eng., 9 (2021) 105284, doi: 10.1016/j.jece.2021.105284.
[40] A. Mukhopadhyay, B.K. Tripathy, A. Debnath, M. Kumar, Enhanced persulfate activated sono-catalytic degradation of brilliant green dye by magnetic $CaFe_2O_4$ nanoparticles: degradation pathway study, assessment of bio-toxicity and

cost analysis, Surf. Interfaces, 26 (2021) 101412, doi: 10.1016/j.surfin.2021.101412.
[41] X. Shen, Z. Liu, J. Li, D. Wu, M. Zhu, L. Yan, G. Mao, X. Ye, R.J. Linhardt, S. Chen, Development of low molecular weight heparin by H_2O_2/ascorbic acid with ultrasonic power and its anti-metastasis property, Int. J. Biol. Macromol., 133 (2019) 101–109.
[42] F. Guenfoud, M. Mokhtari, H. Akrout, Electrochemical degradation of malachite green with BDD electrodes: Effect of electrochemical parameters, Diamond Relat. Mater., 46 (2014) 8–14.
[43] Q. Huang, C. Chen, X. Zhao, X. Bu, X. Liao, H. Fan, W. Gao, H. Hu, Y. Zhang, Z. Huang, Malachite green degradation by persulfate activation with $CuFe_2O_4$@biochar composite: efficiency, stability and mechanism, J. Environ. Chem. Eng., 9 (2021) 105800, doi: 10.1016/j.jece.2021.105800.
[44] Y. Ju, S. Yang, Y. Ding, C. Sun, C. Gu, Z. He, C. Qin, H. He, B. Xu, Microwave-enhanced H_2O_2-based process for treating aqueous malachite green solutions: intermediates and degradation mechanism, J. Hazard. Mater., 171 (2009) 123–132.
[45] C. Peng, L. Chen, X. Wu, X. Wei, A. Tehrim, M. Dai, S. Xu, Identification of adsorption or degradation mechanism for the removal of different ionic dyes with iron-carbon micro-electrolysis process, J. Environ. Chem. Eng., 9 (2021) 105690, doi: 10.1016/j.jece.2021.105690.
[46] Y. Yulizar, D.O.B. Apriandanu, R.I. Ashna, La_2CuO_4-decorated ZnO nanoparticles with improved photocatalytic activity for malachite green degradation, Chem. Phys. Lett., 755 (2020) 137749, doi: 10.1016/j.cplett.2020.137749.
[47] S.S. Sutar, P.J. Patil, A.S. Tamboli, D.N. Patil, O.A. Apine, J.P. Jadhav, Biodegradation and detoxification of malachite green by a newly isolated bioluminescent bacterium *Photobacterium leiognathi* strain MS under RSM optimized culture conditions, Biocatal. Agric. Biotechnol., 20 (2019) 101183, doi: 10.1016/j.bcab.2019.101183.
[48] A.S. Yusuff, I.I. Olateju, O.A. Adesina, TiO_2/anthill clay as a heterogeneous catalyst for solar photocatalytic degradation of textile wastewater: catalyst characterization and optimization studies, Materialia, 8 (2019) 100484, doi: 10.1016/j.mtla.2019.100484.
[49] S.-W. Lv, J.-M. Liu, N. Zhao, C.-Y. Li, F.-E. Yang, Z.-H. Wang, S. Wang, MOF-derived $CoFe_2O_4/Fe_2O_3$ embedded in g-C_3N_4 as high-efficient Z-scheme photocatalysts for enhanced degradation of emerging organic pollutants in the presence of persulfate, Sep. Purif. Technol., 253 (2020) 117413, doi: 10.1016/j.seppur.2020.117413.
[50] K. Mabhouti, M. Karamirad, P. Norouzzadeh, M.M. Golzan, R. Naderali, Measurement of nickel doped zinc oxide NPs resonance frequencies and electromagnetic properties in X-Band, Phys. B Condens. Matter, 602 (2021) 412532, doi: 10.1016/j.physb.2020.412532.
[51] A. Jayachandran, T.R. Aswathy, A.S. Nair, Green synthesis and characterization of zinc oxide nanoparticles using *Cayratia pedata* leaf extract, Biochem. Biophys. Rep., 26 (2021) 100995, doi: 10.1016/j.bbrep.2021.100995.
[52] F. Yaseri Nasab, H. Bahiraei, High photocatalytic activity of magnetically separable ZnO and Ag/ZnO supported on Mg-ferrite nanoparticles, J. Photochem. Photobiol., A, 394 (2020) 112489, doi: 10.1016/j.jphotochem.2020.112489.
[53] P. Gholami, A. Khataee, R.D.C. Soltani, A. Bhatnagar, A review on carbon-based materials for heterogeneous sonocatalysis: fundamentals, properties and applications, Ultrason. Sonochem., 58 (2019) 104681, doi: 10.1016/j.ultsonch.2019.104681.
[54] D. Ayodhya, G. Veerabhadram, Green synthesis of garlic extract stabilized Ag@CeO_2 composites for photocatalytic and sonocatalytic degradation of mixed dyes and antimicrobial studies, J. Mol. Struct., 1205 (2020) 127611, doi: 10.1016/j.molstruc.2019.127611.
[55] N. Jalili-Jahani, F. Rabbani, A. Fatehi, T. Musavi Haghighi, Rapid one-pot synthesis of Ag-decorated ZnO nanoflowers for photocatalytic degradation of tetracycline and product analysis by LC/APCI-MS and direct probe ESI-MS, Adv. Powder Technol., 32 (2021) 3075–3089.
[56] G. Wang, X. Ma, J. Liu, L. Qin, B. Li, Y. Hu, H. Cheng, Design and performance of a novel direct Z-scheme $NiGa_2O_4/CeO_2$ nanocomposite with enhanced sonocatalytic activity, Sci. Total Environ., 741 (2020) 140192, doi: 10.1016/j.scitotenv.2020.140192.
[57] N. Khoshnamvand, A. Jafari, B. Kamarehie, A. Mohammadi, M. Faraji, Removal of malachite green dye from aqueous solutions using zeolitic imidazole framework-8, Environ. Process., 6 (2019) 757–772.
[58] Q. Ren, C. Kong, Z. Chen, J. Zhou, W. Li, D. Li, Z. Cui, Y. Xue, Y. Lu, Ultrasonic assisted electrochemical degradation of malachite green in wastewater, Microchem. J., 164 (2021) 106059, doi: 10.1016/j.microc.2021.106059.
[59] I. Hasan, A. Bassi, K.H. Alharbi, I.I. Bin Sharfan, R.A. Khan, A. Alslame, Sonophotocatalytic degradation of malachite dreen by nanocrystalline chitosan-ascorbic Acid@$NiFe_2O_4$ spinel ferrite, Coatings, 10 (2020) 1200, doi: 10.3390/coatings10121200.
[60] P. Das, P. Debnath, A. Debnath, Enhanced sono-assisted adsorptive uptake of malachite green dye onto magnesium ferrite nanoparticles: kinetic, isotherm and cost analysis, Environ. Nanotechnol. Monit. Manage., 16 (2021) 100506, doi: 10.1016/j.enmm.2021.100506.